Journal of the Mechanical Behavior of Biomedical Materials 74 (2017) 189–194

Contents lists available at ScienceDirect

Journal of the Mechanical Behavior of Biomedical Materials

journal homepage: www.elsevier.com/locate/jmbbm

# Functional trade-off between strength and thermal capacity of dermal armor: Insights from girdled lizards

Chris Broeckhoven[a,b,*], Anton du Plessis[c], Cang Hui[b,d]

[a] Department of Botany & Zoology, Stellenbosch University, Private Bag X1, Matieland, 7602 Stellenbosch, South Africa
[b] Theoretical Ecology Group, Department of Mathematical Sciences, Stellenbosch University, Private Bag X1, Matieland, 7602 Stellenbosch, South Africa
[c] CT Scanner Facility, Central Analytical Facilities, Stellenbosch University, Matieland, 7602 Stellenbosch, South Africa
[d] Theoretical and Physical Biosciences, African Institute for Mathematical Sciences, Cape Town 7945, South Africa

ARTICLE INFO

*Keywords:*
Biomimicry
Osteoderm
Micro-computed tomography
Stress simulation
Thermoregulation

ABSTRACT

The presence of dermal armor is often unambiguously considered the result of an evolutionary predator-prey arms-race. Recent studies focusing predominantly on osteoderms – mineralized elements embedded in the dermis layer of various extant and extinct vertebrates – have instead proposed that dermal armor might exhibit additional functionalities besides protection. Multiple divergent functionalities could impose conflicting demands on a phenotype, yet, functional trade-offs in dermal armor have rarely been investigated. Here, we use high-resolution micro-computed tomography and voxel-based simulations to test for a trade-off between the strength and thermal capacity of osteoderms using two armored cordylid lizards as model organisms. We demonstrate that high vascularization, associated with improved thermal capacity might limit the strength of osteoderms. These results call for a holistic, cautionary future approach to studies investigating dermal armor, especially those aiming to inspire artificial protective materials.

## 1. Introduction

Through millions of years of evolution, nature has unfolded an array of armor types in the animal kingdom. Segmented dermal armors such as osteoderms, bony elements entrenched within the dermis, constitute the most commonly documented type (reviewed in Vickaryous and Sire, 2009) and are present in a variety of extinct and extant animals including dinosaurs (e.g. Farlow et al., 1976; Curry Rogers et al., 2011), crocodilians (e.g. Seidel, 1979; Sun and Chen, 2013; Chen et al., 2014), lizards (e.g. Broeckhoven et al., 2015) and armadillos (e.g. Chen et al., 2011; Krmpotic et al., 2015). Osteoderms have a flexible yet impact resistant nature: robust individual segments anchored by Sharpey's fibres (Chen et al., 2011) or associated with interlocking sutures (Chen et al., 2015) provide flexibility to the underlying musculature while retaining the integrity of the skin upon fracture (Chintapalli et al., 2014). It is often unambiguously assumed that these morphological characteristics are the resultant of an evolutionary predator-prey arms-race that, over time, led to the selection of optimal phenotypes (Yang et al., 2013; Chintapalli et al., 2014). On the contrary, osteoderms have been proposed to exhibit a variety of functionalities in addition to protection, including locomotion (Dilkes and Brown, 2007), mineral storage (Curry Rogers et al., 2011; Dacke et al., 2015), and thermoregulation (Farlow et al., 1976, 2010; Seidel, 1979). In nature, the mechanisms underlying these requirements do not evolve in isolation from one another but instead selection favors coordination with other mechanisms and facilitates the functioning thereof (Buss et al., 1998). The coordination process, however, necessarily entails compromises, such as functional trade-offs among mechanisms imposed by conflicting functional requirements, and appears to place strong constraints on phenotypic trait evolution (Rivera and Stayton, 2011; Li et al., 2015).

Despite the abundance of anecdotal evidence suggesting a multifunctional nature of osteoderms, no study to date has focused on functional trade-offs. The extensive variation in osteoderm expression present in girdled lizards (Squamata: Cordylidae) (Broeckhoven et al., 2015, 2016) provides a unique opportunity to address this issue. Here, we test the hypothesis that dermal armor is constrained by a trade-off between strength and thermal capacity, by examining the morphology, mechanical behavior and thermal capacity of dorsal osteoderms in two heavily armored girdled lizards – the armadillo lizard (*Ouroborus cataphractus*) and giant girdled lizard (*Smaug giganteus*) (Fig. 1) – using micro-computed tomography (micro-CT) and voxel-based simulations.

* Corresponding author at: Department of Botany & Zoology, Stellenbosch University, Private Bag X1, Matieland, 7602 Stellenbosch, South Africa.
*E-mail address:* cbroeck@sun.ac.za (C. Broeckhoven).

http://dx.doi.org/10.1016/j.jmbbm.2017.06.007
Received 25 April 2017; Received in revised form 4 June 2017; Accepted 6 June 2017
Available online 07 June 2017

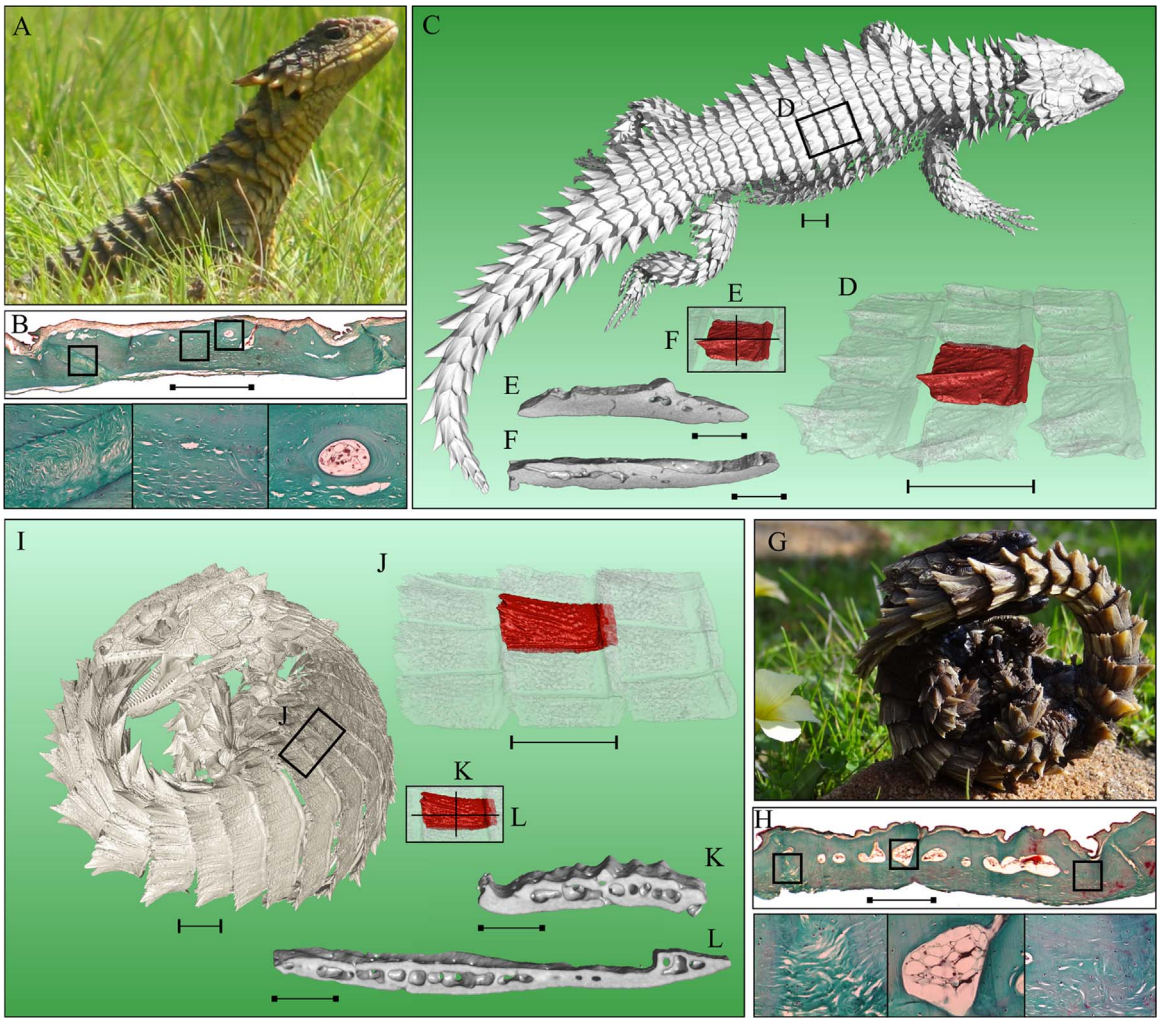


**Fig. 1.** *Smaug giganteus* – A. adult individual; – B. Histological section of dorsal osteoderm in transversal plane with details of Sharpey's fibres, vascular canal encircled with laminar bone and bone microarchitecture; – C. 3D-rendered image of *S. giganteus* showing the extent of osteoderm distribution (data taken from Broeckhoven et al., 2016); – D. Section of dorsal skin highlighting the osteoderm used for morphological analyses and simulations; – E, F. Sections of dorsal osteoderm in transversal and longitudinal view, respectively. *Ouroborus cataphractus* – G. Adult individual; – H. Histological section of dorsal osteoderm in transversal plane with details of Sharpey's fibres, vascular canal showing large adipocytes and bone microarchitecture; I. – 3D-rendered image of live *O. cataphractus* displaying tail-biting behavior (data taken from Broeckhoven et al., 2017); J. Section of dorsal skin highlighting the osteoderm used for morphological analyses and simulations; – K, L. Sections of dorsal osteoderm in transversal and longitudinal view, respectively. Scale bars: (|▬|) 10 mm, (▬▬) 1 mm. Photo copyrights; *S. giganteus*: © Llewellyn & Elzette Angus.

## 2. Methods

### 2.1. Study organisms

Girdled lizards are a family of predominantly rock-dwelling sit-and-wait foraging lizards endemic to sub-Saharan Africa (Mouton and Van Wyk, 1997). Although all members of the family possess (to varying degrees) spines and osteoderms, elaborated body armor evolved convergently in only two species, namely *O. cataphractus* and *S. giganteus* (Broeckhoven et al., 2016; Fig. 1). *Ouroborus cataphractus* inhabits hot, arid environments, characteristic of the Succulent Karoo biome in the western parts of South Africa (Shuttleworth et al., 2013). While most Cordylidae have a generalist insectivorous diet, *O. cataphractus* has specialized in exploiting harvester termites (*Microhodotermes viator*) at the foraging ports of termite nests, considerable distances away from the safety of the rock-crevice. Broeckhoven et al. (2015) postulated that these foraging excursions imply an increased risk of mortality to predation (presumably by small grey mongoose, *Herpestes pulverulentus*; Broeckhoven and Mouton, 2015), which in turn favored the evolution of elaborated body armor in this species. In contrast, *S. giganteus* inhabits the Highveld grasslands of east-central South Africa, typified by cold winters with frost (Van Wyk, 1992). Although most Cordylidae are rock-dwellers, *S. giganteus* reverted to a terrestrial lifestyle and makes use of self-excavated burrows (Mouton and Van Wyk, 1997). Yellow mongoose (*Cynictis penicillata*) and suricates (*Suricata suricatta*), both burrowing predators, are particularly abundant in areas inhabited by *S. giganteus* (Van Wyk, 1992; Broeckhoven personal observations), hence these predators can be considered the main selective pressure for the evolution of elaborated body armor in this species.

The two species are therefore suitable model organisms to test our proposed hypothesis, because both are subjected to similar predation pressure (i.e., exerted by mongooses) associated with their unique lifestyles, yet inhabit contrasting climatic environments.

### 2.2. Sample preparation and micro-CT scanning

Micro-computed tomography (micro-CT) was applied to provide full 3D image datasets of the osteoderms using a GE Phoenix v|tome|x L240 dual tube CT instrument (Phoenix X-ray; General Electric Sensing & Technologies, Wunstorf, Germany) located at the CT facility, Stellenbosch University (du Plessis et al., 2016). Eighteen dorsal sections of the skin measuring approximately 20 × 13 mm and consisting of three rows of three joining osteoderms (Fig. 1 D, J) were excised from the trunk region of adult preserved specimens of *O. cataphractus* and *S.*

*giganteus* housed at the Ellerman Collection, Stellenbosch University. Dorsal osteoderms from the trunk region were specifically chosen because they protect the underlying organs and because this region is more likely to be targeted by predators during attack. The dorsal sections were dried for 24 h after removal of the β-keratin layer, and scanned at 160 kV, 90 μA, with 2000 images acquired in steps during one full rotation of the sample. A spatial resolution of 20 μm was obtained in the micro-CT images. We aimed to obtain the best possible quality for biological samples following the guidelines outlined by du Plessis et al. (2017). Acquired data sets were reconstructed with the system-supplied software, producing 3D data sets which were subsequently analyzed using Volume Graphics VGStudioMax 3.0 (Volume Graphics, Heidelberg, Germany).

Prior to the analyses, a single osteoderm measuring approximately 7 × 4 mm and located in the center of the excised dorsal section was digitally segmented from the neighboring osteoderms, using the following method: Firstly, an adaptive Gauss filter (default parameters) was used for initial noise reduction. Secondly, an advanced surface determination function was applied to accurately determine the edge of the bone material relative to lower density material (e.g. skin, mounting material). If necessary, a single closing function was applied to remove any remaining small dense particles from the scan, followed by a surface determination based on the above “closed” image data. Thirdly, to isolate the individual osteoderms, a region growing tool was applied to the selected osteoderm, and this region (which includes joining osteoderms) was closed using a closing operation, with a 2-voxel value. This process removes limited material from the osteoderm and separates osteoderms from one another. Finally, an advanced surface determination was applied to the isolated osteoderm with a variable search distance to allow the edge to be determined accurately. Once selected, the individual osteoderm was extracted to be used for subsequent analyses.

### 2.3. Morphological analyses of osteoderm structure

To visualize and quantify differences or similarities among thicknesses of osteoderm tissue in the two species, a wall thickness analyses was performed. This is a standard analysis tool which starts at every surface element and searches in a 30 degree angle for a nearby surface element, measuring the minimum distance to this opposite “wall” (Fig. 2A).

To obtain information on the distribution and connectivity of pores and to quantify the pore sizes (~ degree of vascularization), while assisting in visualization of the pore network, the DEFECT ANALYSIS function was used (Volume Graphics GmbH, 2017). Firstly, the surface of an individual osteoderm was segmented, followed by selection of the osteoderm including all air spaces, after erosion of the region to 2-voxels subsurface. By doing so, all edge voxels assigned to air were eliminated. In this newly created volume, air and material was segmented using an advanced surface determination function and a region-of-interest (ROI) selected from this surface, assigned to material. An inverse of this ROI created a separate region assigned to air. At this point, the respective volumes can be determined and the bone volume fraction (BV/TV) calculated.

To provide further insight into the vascularization of osteoderms, the FOAM STRUCTURE analysis was applied to the structures to obtain values for maximum cell volume and maximum strut thickness. This analysis makes use of a sphere-growing algorithm (Volume Graphics GmbH, 2017) which finds the largest sphere in any given pore space, reporting this as the cell volume. The method allows viewing of the largest pore spaces in the osteoderm and comparing maximum size of pore spaces, regardless of connectivity. Moreover, material areas are seen as “struts” and their maximum thickness were also calculated using the sphere-growing method – this gives an indication of the thickest areas, similar to wall thickness analysis but using a different algorithm (Volume Graphics GmbH, 2017).

In addition to the micro-CT analyses, traditional histological techniques were used to provide detailed information on the microarchitecture of osteoderms. For this purpose, a small fragment of dorsal skin was excised from the girdle adjacent to the section used for micro-CT scanning. Skin tissues were decalcified in 3% nitric acid for 24 h, washed and embedded in paraffin wax after dehydration. Transverse sections (8 μm) were prepared and stained using Goldner's Masson trichrome.

### 2.4. Virtual simulations of structural mechanics and thermal conductivity

To model a loading scenario that both lizard species might experience when being attacked by a predator, the STRUCTURAL MECHANICS function was used (Volume Graphics GmbH, 2017). The simulation function assumes a single material with isotropic material parameters and applies a static load. The Young's modulus and Poisson's ratio of the material are used as input parameters, as well as a load application ROI and a fixture ROI. Here, we used a load of 25 N (~ bite force of mongoose; Broeckhoven et al., 2015), load angle orientation perpendicular to the dorsal side of the osteoderm, a simulation cell size of 2 voxels and a maximum of 3000 iterations. The Poisson's ratio was set to 0.3, while an arbitrary value of 0.5 GPa (i.e. close to the value reported for armadillo osteoderms; Chen et al., 2011) was chosen for Young's modulus. The resulting stress distributions can be analyzed in three dimensions and the maximum von Mises stress can be recorded. The technique is a novel approach as it makes use of voxel-based simulation (i.e. performed directly on micro-CT scans) in contrast to the mesh-based simulation approach of finite element analysis. Meshing can be a source of error, especially with micro-CT data, because smoothing is often applied in the process to reduce the large data set size. Nevertheless, the results of the two techniques are highly comparable (du Plessis and Broeckhoven, unpublished data). All simulations were performed using an HP Z820 workstation with 96 GB RAM and an Intel® Xeon® Processor E5-2650 v2 2.6 GHz.

Next, to calculate heat conduction through a two-component material, a thermal conductivity experiment was conducted using the TRANSPORT PHENOMENA module (Volume Graphics GmbH, 2017). The method assumes two stationary materials with different thermal conductivities. Following Hasgall et al. (2017), we used 0.31 W/mK for bone and 0.18 W/mK for yellow bone marrow. The cranial side of the osteoderm was chosen as inlet plane, whereas the caudal side was chosen as outlet plane with a 1 K temperature difference between planes. A simulation cell size of 2 voxels and maximum of 25000 iterations was chosen.

### 2.5. Puncture performance of osteoderms

To verify the results from the stress simulations conducted on the micro-CT scans, additional puncture performance experiments were conducted on single osteoderms. Osteoderms used for the previous analyses were rehydrated for 24 h and mounted on a 1 mm thick section of double sided adhesive tape to imitate the underlying soft tissue. The tip of a canine of a mongoose (*Galerella pulverulenta*) was mounted inside a compression stage (CT500 Microtest Stage, Deben UK Ltd., Suffolk, UK) and pressure was applied at a constant speed (i.e., 1.0 mm/min). The resulting force–penetration curves for the two species were recorded to obtain the force at which osteoderm fracture occurred.

## 3. Results

Micro-CT scans of osteoderms supplemented with histology were used to investigate the morphology of osteoderms. The dorsal armor of both species was composed of osteoderms arranged in an armadillo-like (Krmpotic et al., 2015) organization. Each osteoderm was attached to one another with Sharpey's fibres in the transverse plane (Fig. 1B, H, and Supplementary Fig. S1), thereby forming distinct longitudinally

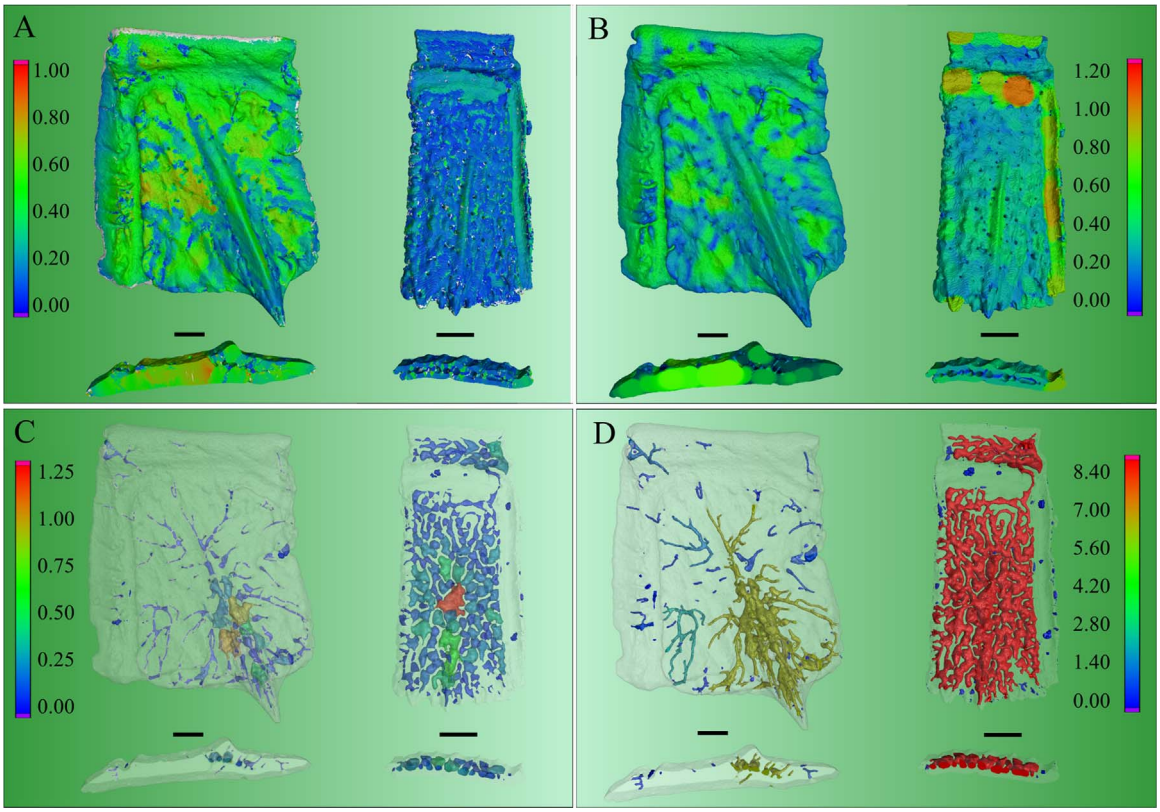


**Fig. 2.** Comparison of morphological analyses conducted on osteoderm micro-CT scans of *S. giganteus* (left) and *O. cataphractus* (right). – A. Wall thickness analysis shows thicker osteoderm tissue in *S. giganteus* with gradient representing the thickness (in mm); – B. Foam structure analysis demonstrates the thicker struts in osteoderms of *S. giganteus*, with gradient representing thickness (in mm); – C. The maximum cell volume (in $mm^3$) of osteoderms was greater in *S. giganteus* due to the presence of a large vascular canal in the keel; – D. Defect analysis illustrates the extensive vascular network in *O. cataphractus*, with gradient representing defect diameter (in mm). Both dorsal view and view of a transversal section of a representative sample are shown. Scale bars: 1 mm.

**Table 1**
Summary of morphological characteristics, mechanical properties and thermal capacity of the dorsal osteoderms of *Ouroborus cataphractus* and *Smaug giganteus*. Values are given as means ± SD.

| | *Ouroborus cataphractus* | *Smaug giganteus* |
|---|---|---|
| Bone volume fraction (BV/TV) | 0.857 ± 0.032 | 0.949 ± 0.021 |
| Average wall thickness (mm) | 0.180 ± 0.022 | 0.295 ± 0.058 |
| Maximum strut thickness (mm) | 1.273 ± 0.522 | 1.643 ± 0.724 |
| Maximum cell volume ($mm^3$) | 0.059 ± 0.027 | 0.081 ± 0.046 |
| Maximum von Mises stress (GPa) | 0.159 ± 0.035 | 0.087 ± 0.020 |
| Thermal Conductivity (W/mK) | 0.287 ± 0.003 | 0.299 ± 0.005 |

imbricated 'girdles' (Fig. 1D, J). In contrast to most tetrapod osteoderms – characterized by a core made up of trabeculae sandwiched between two sheets of compact bone – girdled lizard osteoderms consisted of an outer layer of parallel-fibered bone and inner layer of woven-fibered bone (Fig. 1B, H, and Supplementary Fig. S1). Multiple nutrient foramina led internally to a large vascular network which originated from the keel and spread throughout the osteoderm (Fig. 1, D). The cavities enclosed adipose tissue (i.e. yellow bone marrow) and minute blood vessels, and were encircled by concentric lamellae (Fig. 1B, H, and Supplementary Fig. S1). The BV/TV was lower in *O. cataphractus* than in *S. giganteus* (Mann–Whitney U = 0, $N_1 = N_2 = 9$, $P < 0.001$ two-tailed; Fig. 2C, D; Table 1) as a result of differences in degree of vascularization.

Quantitative stress analyses showed that the maximum von Mises stress of osteoderms after impact of a predator was nearly twice as high in *O. cataphractus* than in *S. giganteus* (Mann–Whitney U = 10, $N_1 = N_2 = 9$, $P < 0.001$ two-tailed; Fig. 3; Table 1). Two models, one including average wall thickness (multiple stepwise regression; $R^2 = 0.792$, $F_{2,16} = 65.8$, $P < 0.001$) and one including wall thickness and maximum strut thickness (multiple stepwise regression; $R^2 = 0.879$, $F_{2,15} = 62.9$, $P < 0.001$) were the best predictors of maximum von Mises stress. The results from additional puncture performance tests corroborated those of the stress simulations and confirmed that fracture occurred at lower force in *O. cataphractus* compared to *S. giganteus* (75.7 ± 23.5 N and 110.4 ± 12.4 N, respectively; Fig. 4).

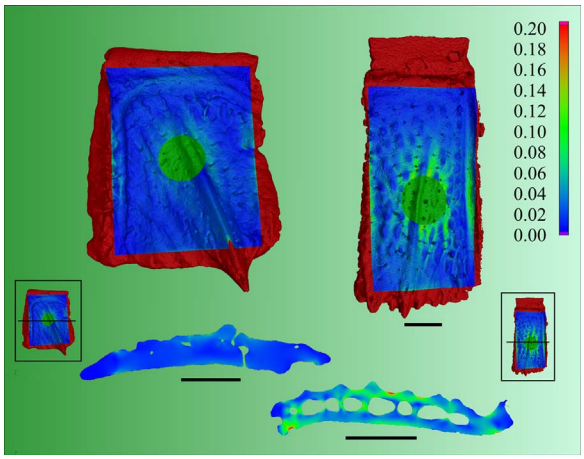


**Fig. 3.** Comparison of stress simulations conducted on osteoderm micro-CT scans of *S. giganteus* (left) and *O. cataphractus* (right). Both dorsal view and view of a transversal section of a representative sample are shown. Gradient represents the maximum von Mises stress (in GPa) after applying a 25 N load. Scale bars: 1 mm.

Virtual thermal conductivity experiments revealed that the thermal conductivity of osteoderms was lower in *O. cataphractus* than in *S. giganteus* (Mann–Whitney U = 9.5, $N1 = N2 = 9$, $P < 0.001$ two-tailed;

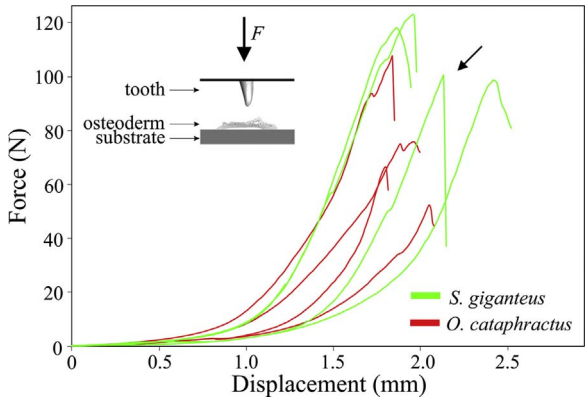


**Fig. 4.** Force-penetration curves into osteoderms by a mongoose tooth. The force required to penetrate the osteoderms of *S. giganteus* is higher than that required to penetrate the osteoderms of *O. cataphractus*. The arrow pointing toward the curve indicates tooth fracture.

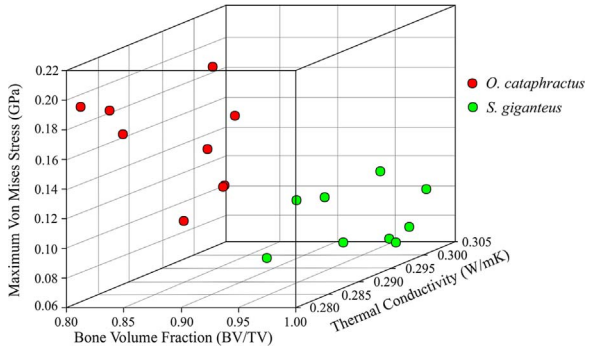


**Fig. 5.** 3D-scatterplot plot showing the relationship between thermal conductivity of osteoderms, maximum von Mises stress during load simulation and bone volume fraction. The osteoderms of *O. cataphractus*, clustered in the upper-left part, are weaker than those *S. giganteus*, clustered in the lower-right part, but have a higher thermal conductivity. Both strength and thermal capacity appear to be a function of the bone volume fraction (~ degree of vascularization). The absence of clear within-species correlations is presumably due to low sample size and/or potential variation among populations from which the specimens originated (see Broeckhoven et al., 2015).

Table 1) and was best predicted by BV/TV (multiple stepwise regression; $R^2 = 0.901$, $F_{1,16} = 155.8$, $P < 0.001$; Fig. 5). Furthermore, a negative correlation was present between thermal conductivity and maximum von Mises stress (Spearman rank correlation: $\rho = -0.69$, $N = 18$, $P = 0.001$; Fig. 5). The lack of correlation within each species (Spearman rank correlation: *O. cataphractus*, $\rho = -0.24$, $N = 9$, $P = 0.53$; *S. giganteus*, $\rho = -0.27$, $N = 9$, $P = 0.49$; Fig. 5) was likely a result of the relatively low sample sizes for each species. Unfortunately, the destructive sampling method and species' conservation status prevented us from obtaining a larger sample size.

## 4. Discussion

While it has been widely assumed that osteoderms serve to protect prey against predators (Broeckhoven et al., 2015), anecdotal evidence suggests that osteoderms comprise multiple functionalities (Seidel, 1979; Dilkes and Brown, 2007; Curry Rogers et al., 2011; Dacke et al., 2015; Vickaryous et al., 2015) including thermoregulation, especially among poikilotherms (Farlow et al., 1976, 2010; Seidel, 1979). It is unlikely that organisms can simultaneously optimize multiple functions, hence the phenotype should reflect the constraints imposed by conflicting morphological demands (Buss et al., 1998).

Despite the convergent evolution in body armor (Broeckhoven et al., 2016), presumably in response to high terrestrial predation pressure associated with a unique lifestyle (Van Wyk, 1992; Broeckhoven et al., 2015), our results indicate the presence of significant interspecific differences in the strength of osteoderms (Figs. 3, 4). These differences in strength might be related to the need for improved thermal capacity: while vascularization throughout the osteoderms could regulate heat absorption and transfer during thermoregulation by vasoconstriction and vasodilation (Farlow et al., 1976, 2010), adipose tissue present in the trabeculae might serve as thermal insulator (Krmpotic et al., 2015). The low thermal conductivity of *O. cataphractus* osteoderms and the extensive vascular network might provide individuals of this species with a significant thermal advantage under semi-desert conditions (Broeckhoven and Mouton, 2015). Indeed, cooling (and presumably heating) rates in *O. cataphractus* are significantly lower than those of similarly sized lizards (Broeckhoven et al., 2017). However, the accompanying changes in microarchitecture appear to lead to high von Mises stress upon impact and ultimately lower the strength of osteoderms. As a result, a trade-off appears to exist between thermoregulatory capacity on the one hand, and strength of osteoderms on the other hand.

The performance cost resulting from competing demands on osteoderms seem to be mitigated by compensatory changes in other life history characteristics. In *S. giganteus*, hibernation and the use of well-insulated self-excavated burrows (Van Wyk, 2000) appears to eliminate the need for improved thermal capacity. In *O. cataphractus* tail-biting behavior (Fig. 1), appears to have evolved to minimize the consequences of this trade-off: predators (i.e. mongooses) are required to maximize their gape, resulting in a decrease in bite force, thereby rendering the defence of *O. cataphractus* stronger than what is theoretically predicted (Broeckhoven et al., 2015).

The understanding of segmented dermal armor, such as osteoderms, is important as it may provide a basis for new synthetic, yet bioinspired, armor materials (Yang et al., 2013; Chintapalli et al., 2014). Animals that possess some form of natural body armor have been the focus of a growing number of biomimetic studies that explore the fracture or puncture resistance of armor (Chen et al., 2011; Sun and Chen, 2013; Yang et al., 2013; Chen et al., 2014). Our results suggest that osteoderms might not have evolved to fulfill a protective role solely, but instead are subjected to multiple selective pressures and are shaped by trade-offs among multiple functions. Understanding natural body armor in a biological context, rather than isolating its protective nature, is pivotal to the advancement of future studies, especially those focusing on the biomechanical or biomimetic aspects of natural body armor. In light of this, the mechanisms, either behavioral (Broeckhoven et al., 2015) or morphological (Rivera and Stayton, 2011), used by organisms to counter negative effects of trade-offs must be taken into consideration.

## Acknowledgements

We are grateful to S.G. le Roux for his assistance with the micro-CT scanning and to P.L.F.N. Mouton for allowing us to make use of the specimens housed in the Ellerman Collection, Stellenbosch University. We also wish to thank M. J. Buehler, the Editor, and two anonymous reviewers for their comments on an earlier version of the manuscript. This research was supported by an NRF South Africa Grant (81825 and 76912) issued to C. Hui and the Australian Research Council (Discovery Project DP150103017).

## Appendix A. Supporting information

Supplementary data associated with this article can be found in the online version at http://dx.doi.org/10.1016/j.jmbbm.2017.06.007.

## References

Broeckhoven, C., Mouton, P.L.F.N., 2015. Some like it hot: camera traps unravel the effects of weather conditions and predator presence on the activity levels of two lizards. PLoS One 10, e0137428.

Broeckhoven, C., Diedericks, G., Mouton, P.L.F.N., 2015. What doesn't kill you might make you stronger: functional basis for variation in body armour. J. Anim. Ecol. 84, 1213–1221.
Broeckhoven, C., Diedericks, G., Hui, C., Makhubo, B.G., Mouton, P.L.F.N., 2016. Enemy at the gates: rapid defensive trait diversification in an adaptive radiation of lizards. Evolution 70 [2647-2645].
Broeckhoven, C., du Plessis, A., le Roux, S.G., Mouton, P.L.F.N., Hui, C., 2017. Beauty is more than skin deep: a non-invasive protocol for *in vivo* anatomical study using micro-CT. Methods Ecol. Evol. 8, 358–369.
Buss, D.M., Haselton, M.G., Shackelford, T.K., Bleske, A.L., Wakefield, J.C., 1998. Adaptations, exaptations, and spandrels. Am. Psychol. 53, 533.
Chen, I.H., Kiang, J.H., Correa, V., Lopez, M.I., Chen, P.-Y., McKittrick, J., Meyers, M.A., 2011. Armadillo armor: mechanical testing and micro-structural evaluation. J. Mech. Behav. Biomed. Mater. 4, 713–722.
Chen, I.H., Yang, W., Meyers, M.A., 2014. Alligator osteoderms: mechanical behavior and hierarchical structure. Mater. Sci. Eng. C 35, 441–448.
Chen, I.H., Yang, W., Meyers, M.A., 2015. Leatherback sea turtle shell: a tough and flexible biological design. Acta Biomater. 28, 2–12.
Chintapalli, R.K., Mirkhalaf, M., Dastjerdi, A.K., Barthelat, F., 2014. Fabrication, testing and modeling of a new flexible armor inspired from natural fish scales and osteoderms. Bioinspiration Biomimimetics 9, 036005.
Curry Rogers, K., D'Emic, M., Rogers, R., Vickaryous, M., Cagan, A., 2011. Sauropod dinosaur osteoderms from the Late Cretaceous of Madagascar. Nat. Commun. 2, 564.
Dacke, C.G., Elsey, R.M., Trosclair, P.L., Sugiyama, T., Nevarez, J.G., Schweitzer, M.H., 2015. Alligator osteoderms as a source of labile calcium for eggshell formation. J. Zool. 297, 255–264.
Dilkes, D., Brown, L.E., 2007. Biomechanics of the vertebrae and associated osteoderms of the early Permian amphibians *Cacops aspidephorus*. J. Zool. 271, 396–407.
Du Plessis, A., le Roux, S.G., Guelpa, A., 2016. The CT scanner facility at Stellenbosch University: an open access X-ray computed tomography laboratory. Nucl. Instrum. Methods Phys. Res. Sect. B: Beam Interact. Mater. At. 384, 42–49.
Du Plessis, A., Broeckhoven, C., Guelpa, A., le Roux, S.G., 2017. Laboratory X-ray micro-computed tomography: a user guideline for biological samples. Gigascience 6, 1–11.
Farlow, J.O., Thompson, C.V., Rosner, D.E., 1976. Plates of the dinosaur Stegosaurus: forced convection heat loss fins? Science 192, 1123–1125.
Farlow, J.O., Hayashi, S., Tattersall, G.J., 2010. Internal vascularity of the dermal plates of *Stegosaurus* (Ornithischia, Thyreophora). Swiss J. Geosci. 103, 173–185.
Hasgall, P.A., E. Neufeld, M.C. Gosselin, A. Klingenböck, N. Kuster. 2017. IT'IS Database for Thermal and Electromagnetic Parameters of Biological Tissues, Version 3.0. ⟨http://dx.doi.org/10.13099/VIP21000-03-0⟩. Available at ⟨www.itis.ethz.ch/database⟩. [Accessed 10 January 2017].
Krmpotic, C.M., Ciancio, M.R., Carlini, A.A., Castro, M.C., Scarano, A.C., Barbeito, C.G., 2015. Comparative histology and ontogenetic change in the carapace of armadillos (Mammalia: Dasypodidae). Zoomorphology 134, 601–616.
Li, L., Connors, M.J., Kolle, M., England, G.T., Speiser, D.I., Xiao, X., Aizenberg, J., Ortiz, C., 2015. Multifunctionality of chiton biomineralized armor with an integrated visual system. Science 350, 952–956.
Mouton, P.L.F.N., van Wyk, J.H., 1997. Adaptive radiation in cordyliform lizards: an overview. Afr. J. Herpetol. 46, 78–88.
Rivera, G., Stayton, C.T., 2011. Finite element modeling of shell shape in the freshwater turtle *Pseudemys concinna* reveals a trade-off between mechanical strength and hydrodynamic efficiency. J. Morphol. 272, 1192–1203.
Seidel, M.R., 1979. The osteoderms of the American alligator and their functional significance. Herpetologica 35, 375–380.
Shuttleworth, C., Mouton, P.L.F.N., Van Niekerk, A., 2013. Climate and the evolution of group-living behaviour in the armadillo lizard (*Ouroborus cataphractus*). Afr. Zool. 48, 367–373.
Sun, C.-Y., Chen, P.-Y., 2013. Structural design and mechanical behavior of alligator (*Alligator mississippiensis*) osteoderms. Acta Biomater. 9, 9049–9064.
Van Wyk, J.H., 1992. Life History and Physiological Ecology of the Lizard, *Cordylus giganteus* [PhD Dissertation]. University of Cape Town.
Van Wyk, J.H., 2000. Seasonal variation in stomach contents and diet composition in the large girdled lizard, *Cordylus giganteus* (Reptilia: Cordylidae) in the Highveld grasslands of the northeastern free state, South Africa. Afr. Zool. 35, 9–27.
Vickaryous, M.K., Meldrum, G., Russell, A.P., 2015. Armored geckos: a histological investigation of osteoderm development in Tarentola (Phyllodactylidae) and Gekko (Gekkonidae) with comments on their regeneration and inferred function. J. Morph. 276, 1345–1357.
Vickaryous, M.K., Sire, J.Y., 2009. The integumentary skeleton of tetrapods: origin, evolution, and development. J. Anat. 214, 441–464.
Volume Graphics GmbH. 2017. VGStudio Max 3.0 Reference Manual. Online: ⟨http://www.volumegraphics.com⟩.
Yang, W., Chen, I.H., Gludovatz, B., Zimmermann, E.A., Ritchie, R.O., Meyers, M.A., 2013. Natural flexible dermal armor. Adv. Mater. 25, 31–48.